# Tactile Discrimination in a Soft Octopus-Inspired Robot

Eleanore J. Kirshner[1], Alina Yuan[2], Jayce Spurgiasz[3], Harrison Espino[4], and Jeffrey L. Krichmar[4,5(✉)]

[1] Department of Mechanical and Aerospace Engineering, University of California, Irvine, CA 92697, USA
ekirshne@uci.edu

[2] Department of Art, University of California, Irvine, CA 92697, USA
yuanax@uci.edu

[3] Department of Computer Science and Engineering, University of California, Irvine, CA 92697, USA
jspurgia@uci.edu

[4] Department of Computer Science, University of California, Irvine, CA 92697, USA
espinoh@uci.edu

[5] Department of Cognitive Sciences, University of California, Irvine, CA 92697, USA
jkrichma@uci.edu

**Abstract.** Octopuses are highly intelligent creatures with remarkable dexterity. Their soft arms operate independently, each covered with numerous chemotactile sensors. Inspired by the octopus, we created the OctoBot, a mobile biomimetic robot with four flexible arms, each embedded with a pressure sensor. The OctoBot is enclosed within an interactive shell containing an LED matrix that communicates its output to an observer in real time, much like the octopus's expressive skin. An important goal of this work was to build a fully integrated, self-contained robotic system capable of onboard sensing and decision-making, using primarily off-the-shelf and low-cost materials. Using t-SNE and hierarchical clustering of the measured sensor signals, texture emerged as the dominant property distinguishing nine objects with varying physical properties. A Random Forest classifier achieved over 90% accuracy when grouping these objects into the three texture categories identified earlier, compared to lower accuracy when classifying all nine objects individually. This classifier was deployed directly onto the robot's onboard microcontroller for real-time classification without external computation.

**Keywords:** Manipulation · Neurorobotics · Octopus · Soft Robotics · Tactile Discrimination

## 1 Introduction

Octopuses, with their sophisticated problem-solving and discrimination abilities, have become a model organism for cognition [11,12]. What sets this invertebrate

© The Author(s), under exclusive license to Springer Nature Switzerland AG 2027
O. Brock et al. (Eds.): SAB 2026, LNAI 16965, pp. 335–346, 2027.
https://doi.org/10.1007/978-3-032-39953-3_27

apart from other intelligent animals is its arms. The octopus' eight arms have distributed nervous systems that allow them to act independently [5]. Each arm is embedded with numerous suckers that have chemotactile sensors [8,14]. This organism, with its soft body and flexible arms, has inspired robot designs, especially in the field of soft robotics [4,6]. Such robots could advance applications such as deep sea exploration [7], where manipulation and mobility are important.

Taking inspiration from the octopus and soft robotics, we introduce the OctoBot: a biomimetic robot focused on manipulation and tactile discrimination. We designed soft, flexible arms embedded with pressure sensors capable of grasping objects of varying size and shape. Like the octopus, the arms can sense and discriminate between objects through touch. An important goal of this work was to create this system with mainly off-the-shelf parts and readily available materials. Similar to our prior work on cephalopod neurorobotics [9], we aimed to construct a fully integrated system: a physically embodied robot capable of autonomous sensing and onboard decision-making without reliance on external computation. The OctoBot is a mobile platform with multiple arms that move independently. Because octopuses camouflage and signal with their skin, the OctoBot has a shell embedded with an LED array. In the present work, the LED array displays the robot's classification output in real time, signaling the detected tactile class to an observer.

The main contributions of this work are:

1. Biomimetic octopus robot with four independently actuated arms and an interactive shell capable of onboard sensing and decision-making.
2. Flexible, compliant arms constructed entirely from off-the-shelf components and low-cost 3D-printed parts, demonstrating that soft robotic platforms need not rely on specialized or expensive fabrication.
3. Tactile-based object discrimination achieving over 90% accuracy using a single pressure sensor and a lightweight onboard classifier.

## 2 Related Work

Octopus arms are highly flexible because they lack bones and tendons, giving them near-infinite degrees of freedom. This has inspired manipulation solutions using soft materials relevant to the OctoBot's arm design. Magnetic resonance imaging of octopus arm musculature has informed the design of soft arms using silicone rubber [1]. Finite element analysis of candidate designs found that incorporating muscle cross-sectional area variation and an axial core was both the most biomimetic and achieved the largest range of motion. A soft arm linked to a rigid base demonstrated pushing-based locomotion and object grasping using soft silicone material with cables [3]. The octopuses' suckers allow them to manipulate, touch, and taste objects [8], inspiring the creation of suction cup arms to grasp a wide range of objects [17] and motivating our focus on tactile discrimination. Chemoreceptive, photoreceptive, iontronic, piezoelectric, and triboelectric technologies have been used to create bio-inspired sensors [10], and electronic skins mimicking the octopus's ability to change shape and color are an active

area of research [13]. However, these approaches require complex fabrication and exotic materials.

Tactile sensing for soft actuators has also been explored beyond octopus-inspired designs. A microphone embedded inside a soft pneumatic actuator can classify location, force, and material type from the acoustic signature of contact events [18]. This approach was extended to produce a virtual 2D tactile array [15]. RC-delay-based capacitive sensing has enabled multi-point touch localization in 3D-printed objects using only a single wire [2]. Both approaches recover rich tactile information from minimal hardware but require either embedded acoustic transducers or multi-material conductive printing. In contrast, the OctoBot's arms follow the open-source SpiRob design [16], which can be constructed using consumer-grade 3D printers. The arm naturally conforms to a wide range of shapes and sizes, due to tapering similar to the octopus [14]. Since the original SpiRob work did not address sensing, we extended it with a flexible capacitive-resistive pressure sensor strip embedded in each arm, enabling tactile discrimination without the fabrication complexity of prior approaches.

## 3 Methods

### 3.1 Robot Platform

The OctoBot robot base was constructed using the LEGO SPIKE Prime platform, with two motors providing locomotion. The SPIKE Prime Hub was interfaced with a LMS-ESP32 microcontroller board, which served as the primary controller for the tactile classification pipeline (antonsmindstorms.com). The ESP32 was connected to four 35 kg 360° winch servo motors, a flexible resistive pressure sensor strip (Plyon® flex sensors, Tacterion), and a 16×16 NeoPixel LED matrix. The complete robot assembly is shown in Fig. 1. A video of the robot grasping and classifying an object is available online at https://youtu.be/dSuxRjIRubI.

### 3.2 Arm Design and Actuation

Four soft, flexible arms were attached to the servo motors via custom 3D-printed connectors. Each arm was 3D-printed in 95A Shore hardness thermoplastic polyurethane (TPU), a flexible filament suited for repeated bending. The arm followed the SpiRob's open-source design [16] and is 114 mm (4.5 in) in length with 16 articulated sections. Actuation was achieved by routing fishing line through the length of the arm and anchoring it to the servo winch. As the winch retracted the line, the arm curled inward and wrapped around an object. A flexible resistive pressure sensor strip, slotted longitudinally into the arm, captured the distributed pressure profile of the contact event. The tactile sensing assembly is shown in Fig. 2.

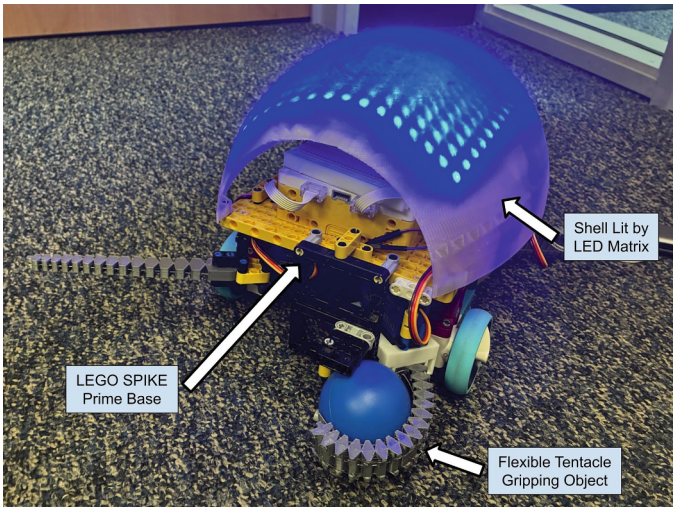



**Fig. 1. OctoBot.** The complete robot system. The LEGO SPIKE Prime base supports four 3D-printed flexible-polymer arms, enclosed in a 3D-printed transparent shell housing the LED matrix display.

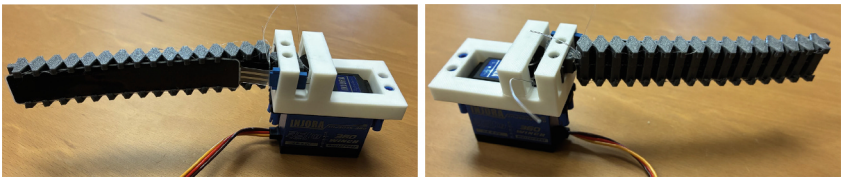


**Fig. 2.** OctoBot arm assembly viewed from two angles. The assembly includes the servo motor, the white 3D-printed connector coupling the arm to the servo motor, and the 3D-printed arm. Each arm is made from 95A TPU and has 16 articulated sections, a routing channel for the fishing line, and a slot for the flexible pressure sensor strip.

### 3.3 Electronics and Sensing

The sensor output was read via the ESP32's analog-to-digital converter (ADC), which converts the sensor's continuous voltage signal into discrete digital values, sampled at 50 ms intervals over an 8 s grip window. The sensor signal was transmitted from the ESP32 to a host PC over USB serial for data logging during the calibration phase, and processed entirely on device during deployment. The electronic subsystem is shown in Fig. 3.

### 3.4 Enclosure and User Interface

The OctoBot shell, which covered the robot base and electronics, was 3D-printed from polyethylene terephthalate glycol (PETG), a rigid filament that prints with high transparency, allowing the internal LED matrix to remain visible. The shell

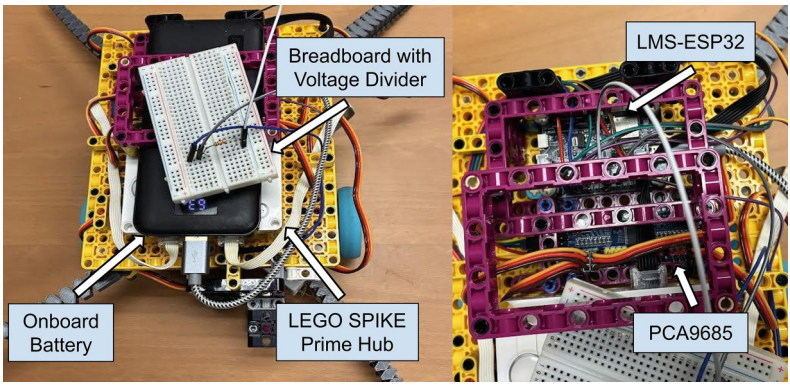



**Fig. 3.** Electronics subsystem. The LEGO SPIKE Prime Hub drives the wheel motors, while the LMS-ESP32 independently controls the four tentacle servos (via a PCA9685 driver), the NeoPixel LED matrix, and the pressure sensor, communicating with the hub as needed. A single onboard battery powers the LMS-ESP32.

housed a 16×16 NeoPixel LED matrix, which displayed the predicted object class as a color to an external observer following each classification, providing real-time visual feedback without requiring a connected display or host computer.

### 3.5 Object Set

The OctoBot's tactile classification performance was evaluated with nine objects having varying physical properties. The full object set, which is shown in Fig. 4, varied in size, texture, and density. During data collection, each object was held stationary at a fixed location in front of the robot. The arm actuated to grab the object for one full grip window, and this process was repeated for 25 trials per object class, resulting in a dataset of 225 labeled trials in total.

### 3.6 Feature Extraction

Two groups of features were extracted and concatenated into a single feature vector. Signal features described the overall shape of the pressure curve: its mean, spread, skewness, rate of change, linear trend, and dominant frequency content via the spectral centroid

$$f_c = \frac{\sum_k \nu_k \cdot |S_k|}{\sum_k |S_k|} \tag{1}$$

where $S_k$ is the discrete Fourier transform of the zero-mean signal and $\nu_k$ is the frequency of the $k$-th bin in Hz. Compression features described how the pressure dropped during contact. These included the depth of compression $p_0 - p_f$, the ratio $p_f/p_0$ relative to the resting value $p_0$, the timing of the drop onset, and the behavior of the signal once it reached a plateau. Prior to classification, all features

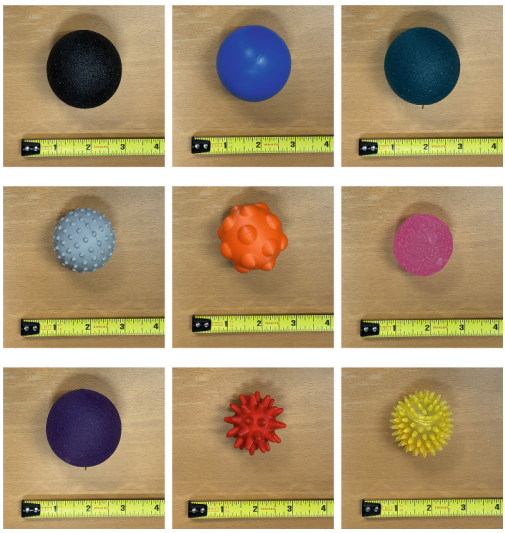


**Fig. 4.** The nine objects used for tactile classification, arranged alphabetically (left to right, top to bottom): black, blue, green, light grey, orange, pink, purple, red, yellow. Objects differed in size (1.5–2.0 in diameter, measured by the ruler shown in each panel), surface texture (smooth to spiky), and material density (gel-like to rigid plastic). Object color was used only for human identification and was not sensed by the OctoBot. (Color figure online)

were scaled to zero mean and unit variance, where $\mu_i$ and $\sigma_i$ are computed over all training trials:

$$\hat{f}_i = \frac{f_i - \mu_i}{\sigma_i} \tag{2}$$

## 4 Results

### 4.1 Sensor Signal Characteristics

The pressure signals as the arm curled around each object showed clear differences between objects. Figure 5 shows the class-mean ADC pressure signals recorded during the 8 s grip window as the arm curled around an object. A clear stratification was visible across object classes: high-texture objects such as red, orange, yellow, and light grey produced early, sustained pressure drops from the resting baseline, while medium-texture objects such as pink, green, purple, and black produced lower drops at a later time. The smooth, blue object showed no pressure drop, indicating that the force was spread over too wide of an area for the sensor to read. This confirms that the flexible pressure strip reliably encodes object texture when the arm curls, with highly textured objects applying a force over a smaller area and generating a greater sensor reading. Figure 6 presents all 25 individual trials per class in a 3×3 grid, with individual runs shown in

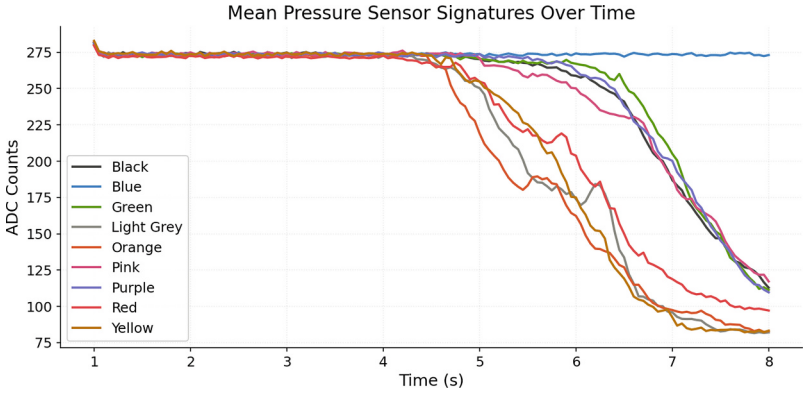



**Fig. 5.** Class-mean ADC pressure signals over the 8 s grip window for all nine object classes, averaged across 25 trials per class. Lower ADC values indicate greater sensor compression. Signals are separated by object texture: highly textured objects produce earlier, larger pressure drops, while the smooth blue object shows almost no drop. (Color figure online)

lighter coloring and trial-to-trial variability indicated by the shaded standard deviation band. Objects with higher surface texture exhibit greater trial-to-trial variability, reflected in wider shading, as irregular surfaces make it difficult to replicate the exact grip orientation across trials. These trials demonstrate that the arm design embedded with a flexible pressure sensor was sufficient to grasp and delineate objects through touch.

### 4.2 Feature Space Visualizations

To further analyze how the OctoBot's arm categorized objects through touch, we applied t-SNE (t-distributed stochastic neighbor embedding), which projects high-dimensional data into two dimensions for visualization, to check whether the extracted features separate by texture without using class labels in the projection itself (Fig. 7). The smooth object (blue) formed a compact, well-separated island at one extreme of the embedding, medium-textured objects (pink, purple, green, black) occupied a central region, and high-textured objects (red, orange, yellow, light grey) congregated toward the right of the figure. The similarly textured objects overlap substantially, forming a dense cluster that reflected their near-identical compression signatures, despite differing markedly in density and size. This overlap confirmed that surface texture was reliably encoded by the 1-dimensional pressure signal.

In addition to the t-SNE, we applied Ward-linkage hierarchical clustering to check if these category groupings were consistent (Fig. 8). The Ward-linkage iteratively merges the most similar classes and reports a linkage distance quantifying their dissimilarity at each merge. The resulting dendrogram reveals a consistent three-group structure separating smooth (blue), high texture (red), and medium

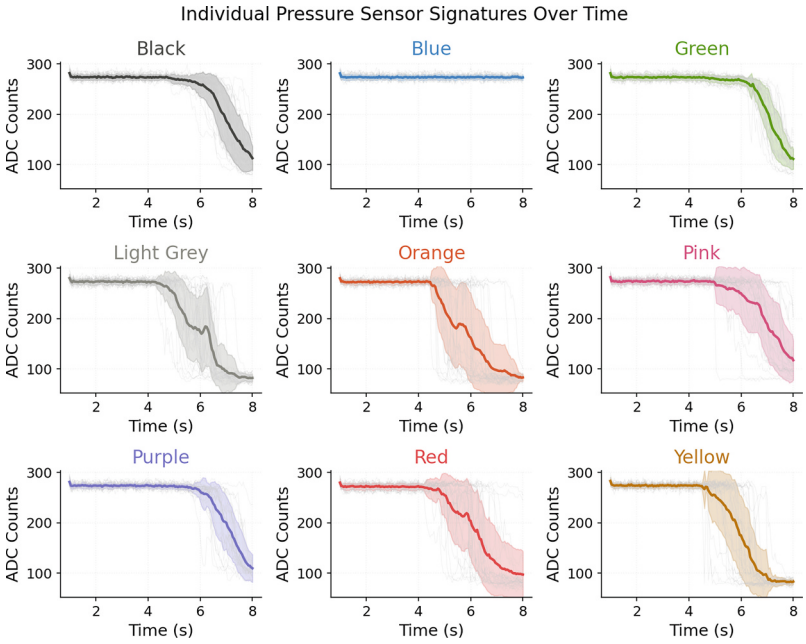



**Fig. 6.** Individual trial fingerprints (faint grey lines, 25 per class) with the class mean (solid line) and ±1 standard deviation (shaded band) for all nine classes. Wider shading indicates greater trial-to-trial variability, which is most pronounced for highly textured objects due to inconsistent grip orientation across trials. (Color figure online)

texture objects (green). The three groups merge only at a much larger linkage distance than any within-group merge, indicating that differences between texture groups dominate over differences among objects within the same group. This data-driven grouping closely matches the groupings observed in the signal characteristics (Fig. 5) and in the t-SNE embedding (Fig. 7).

### 4.3 Classification Performance

Because there was overlap between the nine objects, we further refined the classification system by using a Random Forest classifier. The classifier was trained on standardized feature vectors using 10-fold stratified cross-validation, in which the data is split into 10 class-balanced folds, training on 9 and testing on the held-out fold in turn. Two classification tasks were evaluated: a fine-grained 9-class task, where each object constituted its own class, and a grouped 3-class task, in which objects were assigned to one of three groups based on the hierarchical clustering and t-SNE analysis described in Sect. 4.2:

- **Group A** (high texture): orange, light grey, yellow, red
- **Group B** (medium texture): green, purple, black, pink
- **Group C** (low texture): blue

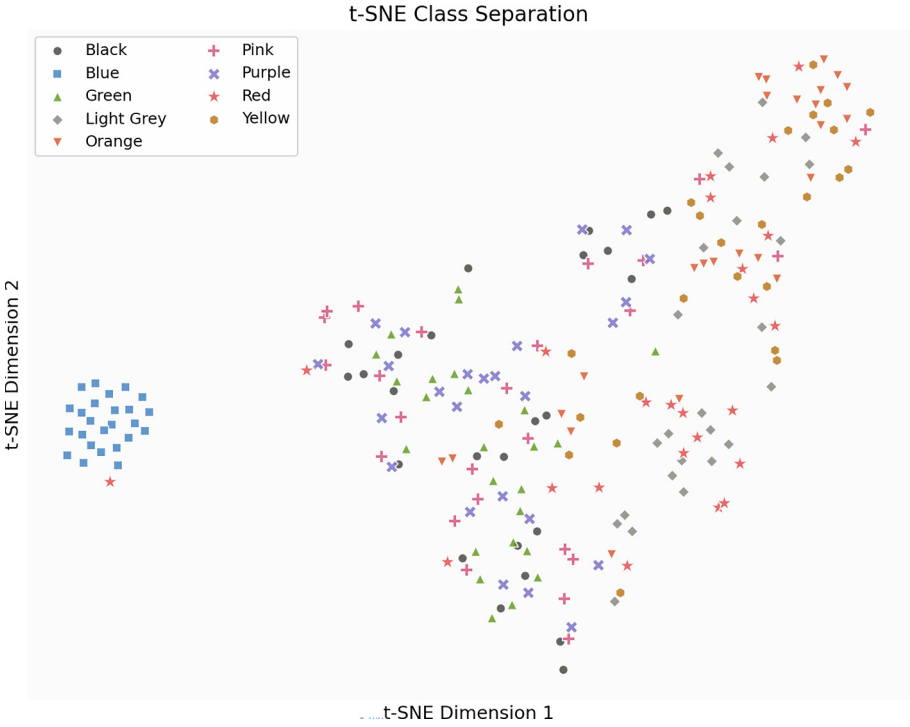



**Fig. 7.** Visualization of object tactile properties with a t-SNE projection. t-SNE reduces the high-dimensional feature space into two dimensions without using class labels. Objects mainly group by texture in this unsupervised projection, despite differing in density and size, supporting the claim that the extracted features primarily encode texture.

The Random Forest classifier was able to classify objects, especially when reduced to three groupings (compare Figs. 9 to 10). The 9-class task achieves a macro-averaged F1-score of 0.329. While modest in absolute terms, this is well above the random baseline of 11.1% for a 9-class problem. Misclassifications are concentrated among objects with similar textures, which are frequently predicted as one another. The grouped task shown in Fig. 10 achieves a macro-averaged F1-score of 0.951, demonstrating that a single pressure sensor embedded in a soft robotic arm can reliably distinguish objects by texture, even when fine-grained per-object classification is not achievable. Taken together, these results show that the OctoBot was able to reliably distinguish tactile classes.

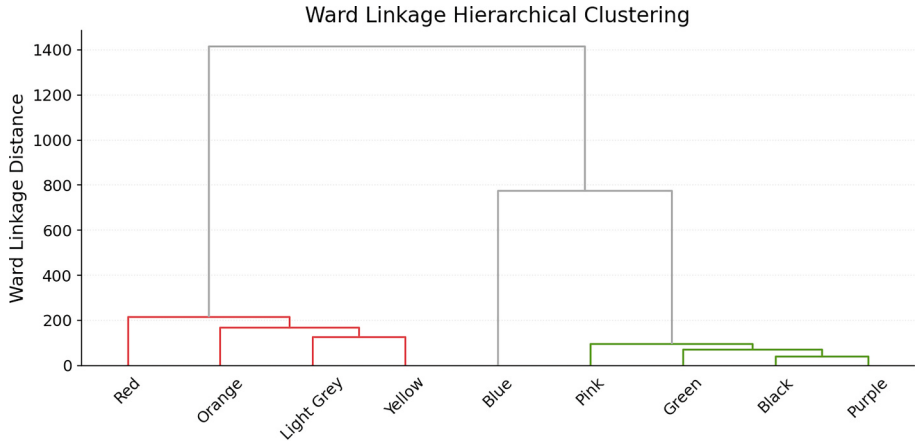



**Fig. 8.** Ward-linkage dendrogram of the nine class-mean signals, where merge height reflects dissimilarity between clusters. Objects merge first within their texture group and only much later across groups, providing independent, data-driven support, consistent with Figs. 5 and 7, that texture is the dominant signal the classifier distinguishes.

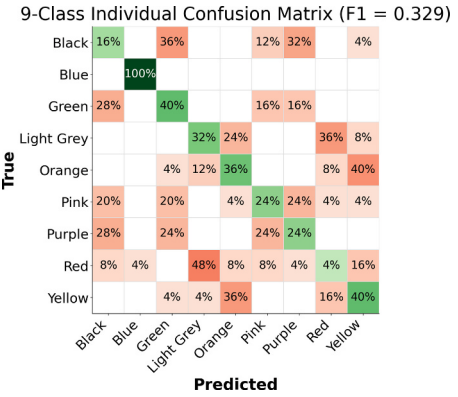



**Fig. 9.** 9-class confusion matrix (Macro F1 = 0.329). Green diagonal cells indicate correct classifications; red off-diagonal cells indicate misclassifications. Dominant errors occur among objects with similar textures. (Color figure online)

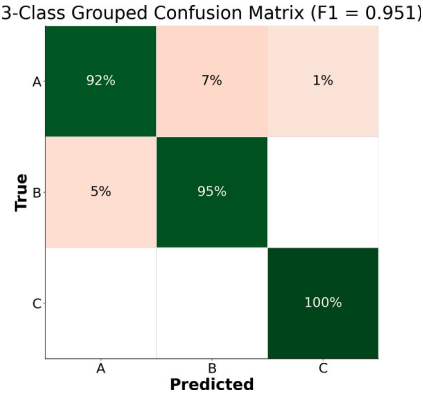



**Fig. 10.** Grouped 3-class confusion matrix (Macro F1 = 0.951), using the texture groups defined in Sect. 4.3. Green diagonal cells indicate correct classifications; red off-diagonal cells indicate misclassifications.

## 5 Discussion and Conclusions

This work introduces the OctoBot, a biomimetic robot inspired by the octopus that features a mobile base, interactive skin, and arms made with soft, compliant

materials. The focus and main contribution of the present paper is to develop a low cost, easily fabricated tactile discrimination system that mimics the octopus.

The compliant arms, each embedded with a pressure sensor, were sufficient for reliable tactile object discrimination through touch alone. The data-driven three-group partition recovered by hierarchical clustering closely matched the physical grouping defined by object properties, validating the feature extraction approach and suggesting that the signal features captured physically meaningful structure. The on-device inference and immediate LED feedback demonstrated that the complete pipeline of sensing, feature extraction, classification, and display was viable for real-time embedded deployment without external computation.

Future work will focus on integrating additional sensing modalities to bridge the current gap in discriminating objects by size and density. Candidate additions include distributed pressure arrays for spatially resolved contact profiles and strain gauges to understand how the material deforms. Together, these extensions are expected to push fine-grained per-object classification substantially beyond the current limitations. In addition, experimental studies comparing human tactile perception to the OctoBot's sensing capabilities are currently underway. These experiments aim to evaluate how accurately the OctoBot can identify, group, and distinguish objects relative to human touch, providing a benchmark for assessing the effectiveness and accuracy of the robot's tactile perception system. The present work is an important step towards a complete neurorobotic system that models these highly intelligent cephalopods.

**Acknowledgments.** This was supported by the UC Irvine California Institute for Telecommunications and Information Technology (CALIT2) in collaboration with the UC Irvine Undergraduate Research Opportunities Program (UROP). The authors thank Ben Dolan of UCI RapidTech for his help with early arm prototypes.

## References

1. Ahmadi, S., et al.: Designing soft arms with octopus-like dexterity: insights from magnetic resonance imaging and finite element analysis. Soft Robo. 21695172251409883 (2026). https://doi.org/10.1177/21695172251409883
2. Bae, S.S., Fujiwara, T., Albers Szafir, D., Do, E., Rivera, M.: Computational design and single-wire sensing of 3D printed objects with integrated capacitive touch-points. In: Proceedings of the ACM Symposium on Computational Fabrication, pp. 1–19. SCF '25 (2025). https://doi.org/10.1145/3745778.3766650
3. Calisti, M., et al.: An octopus-bioinspired solution to movement and manipulation for soft robots. Bioinspir. Biomim. **6**(3), 036002 (2011). https://doi.org/10.1088/1748-3182/6/3/036002
4. Hegde, C., Su, J., Tan, J.M.R., He, K., Chen, X., Magdassi, S.: Sensing in soft robotics. ACS Nano **17**(16), 15277–15307 (2023). https://doi.org/10.1021/acsnano.3c04089
5. Kuuspalu, A., Cody, S., Hale, M.E.: Multiple nerve cords connect the arms of octopuses, providing alternative paths for inter-arm signaling. Curr Biol **32**(24), 5415–5421 e3 (2022). https://doi.org/10.1016/j.cub.2022.11.007

6. Laschi, C., Mazzolai, B.: Lessons from animals and plants: the symbiosis of morphological computation and soft robotics. IEEE Robot. Autom. Mag. **23**(3), 107–114 (2016). https://doi.org/10.1109/MRA.2016.2582726
7. Li, G., et al.: Bioinspired soft robots for deep-sea exploration. Nat. Commun. **14**(1), 7097 (2023). https://doi.org/10.1038/s41467-023-42882-3
8. Olson, C.S., Schulz, N.G., Ragsdale, C.W.: Neuronal segmentation in cephalopod arms. Nat. Commun. **16**(1), 443 (2025). https://doi.org/10.1038/s41467-024-55475-5
9. Pfeiffer, M.A., et al.: Cuttlebot: emulating cuttlefish behavior and intelligence in a novel robot design. In: Brock, O., Krichmar, J. (eds.) From Animals to Animats 17, vol. 14993, pp. 93–105. Lecture Notes in Artificial Intelligence, Springer Nature (2025). https://doi.org/10.1007/978-3-031-71533-4_7
10. Qu, J., et al.: Advanced flexible sensing technologies for soft robots. Adv. Func. Mater. **34**(29), 2401311 (2024). https://doi.org/10.1002/adfm.202401311
11. Schnell, A.K., Amodio, P., Boeckle, M., Clayton, N.S.: How intelligent is a cephalopod? Lessons from comparative cognition. Biol. Rev. **96**(1), 162–178 (2021). https://doi.org/10.1111/brv.12651
12. Schnell, A.K., Clayton, N.S.: Cephalopods: ambassadors for rethinking cognition. Biochem. Biophys. Res. Commun. **564**, 27–36 (2021). https://doi.org/10.1016/j.bbrc.2020.12.062
13. Shih, B., et al.: Electronic skins and machine learning for intelligent soft robots. Sci. Robo. **5**(41), eaaz9239 (2020). https://doi.org/10.1126/scirobotics.aaz9239
14. Sugarman, A., et al.: Long-range neural pathways for octopus chemotactile processing revealed from periphery-to-brain by centimeter-field microct. bioRxiv, p. 2026.01.02.697341 (2026). https://doi.org/10.64898/2026.01.02.697341
15. Wall, V., Brock, O.: A virtual 2D tactile array for soft actuators using acoustic sensing. In: IEEE/RSJ International Conference on Intelligent Robots and Systems (IROS), pp. 10029–10034 (2022). https://doi.org/10.1109/IROS47612.2022.9981225
16. Wang, Z., Freris, N.M., Wei, X.: Spirobs: logarithmic spiral-shaped robots for versatile grasping across scales. Device **3**(4), 100646 (2025). https://doi.org/10.1016/j.device.2024.100646
17. Yue, T., et al.: Embodying soft robots with octopus-inspired hierarchical suction intelligence. Sci. Robo. **10**(102), eadr4264 (2025). https://doi.org/10.1126/scirobotics.adr4264
18. Zöller, G., Wall, V., Brock, O.: Acoustic sensing for soft pneumatic actuators. In: IEEE/RSJ International Conference on Intelligent Robots and Systems (IROS), pp. 6986–6991 (2018). https://doi.org/10.1109/IROS.2018.8594396